

RESEARCH NOTE

Open Access



# Investigation of potential KRASG12D inhibitors: a comparative study between MRTX1133 and natural compounds via computational structural biology approaches

Safiye Merve Bostancioglu<sup>2\*</sup> and Ahmet Acar<sup>1\*</sup>

## Abstract

**Objective** The RAS family, comprising KRAS, NRAS, and HRAS, plays a pivotal role in oncogenesis, dynamically regulating cellular processes through intricate cycling between active and inactive states. Despite recent advancements, direct therapeutic targeting of RAS proteins has proven challenging. Targeting KRASG12D with natural compounds offers a unique therapeutic potential, leveraging the structural diversity and bioactivity of natural compounds. In this study, we investigated the potential of natural products to target oncogenic KRASG12D mutant. Given the higher prevalence of KRASG12D mutations, our study employs structure-based virtual screening and molecular dynamics simulations to identify potential KRASG12D inhibitors within a natural compound library.

**Results** Two natural compounds, NPA019556 and NPA032945, demonstrated strong and stable binding interactions with KRASG12D, surpassing the performance of known inhibitor MRTX1133. After post-molecular dynamics analyses, which encompass Dynamic Cross-Correlation Matrix and Principal Component Analysis, additional evidence suggests that the flexible switch I (residues 30–40) and switch II (residues 58–72) regions demonstrate greater anti-correlation in NPA019556 and NPA032945 compared to MRTX1133 complexed with KRASG12D. These findings highlight the promise of two natural compounds, NPA019556 and NPA032945, as specific KRASG12D inhibitors, paving the way for future and therapeutic development.

**Keywords** Natural products, KRASG12D, Structure-based virtual screening, Molecular dynamics simulation, MRTX1133

\*Correspondence:

Safiye Merve Bostancioglu  
mervebostancioglu@marun.edu.tr  
Ahmet Acar  
acara@metu.edu.tr

<sup>1</sup>Department of Biological Sciences, Middle East Technical University, Universiteler Mah. Dumlupınar Bulvarı 1, Çankaya, Ankara 06800, Turkey

<sup>2</sup>Department of Biology, Faculty of Arts and Sciences, Marmara University, Goztepe Campus, Goztepe, Istanbul 34722, Turkey



© The Author(s) 2025. **Open Access** This article is licensed under a Creative Commons Attribution-NonCommercial-NoDerivatives 4.0 International License, which permits any non-commercial use, sharing, distribution and reproduction in any medium or format, as long as you give appropriate credit to the original author(s) and the source, provide a link to the Creative Commons licence, and indicate if you modified the licensed material. You do not have permission under this licence to share adapted material derived from this article or parts of it. The images or other third party material in this article are included in the article's Creative Commons licence, unless indicated otherwise in a credit line to the material. If material is not included in the article's Creative Commons licence and your intended use is not permitted by statutory regulation or exceeds the permitted use, you will need to obtain permission directly from the copyright holder. To view a copy of this licence, visit <http://creativecommons.org/licenses/by-nc-nd/4.0/>.

## Introduction

The RAS family of GTPases, encompassing KRAS, NRAS, and HRAS, has emerged as pivotal oncogenes in human cancers [1, 2]. Functioning as molecular switches, these proteins dynamically transition between active and inactive states, exerting profound influence on mediating cellular processes [3]. Activation of RAS proteins occurs upon binding to GTP, while deactivation is facilitated by GDP binding [4]. This intricate cycling is rigorously regulated by multi-domain proteins, specifically guanine nucleotide exchange factors (GEFs) and GTPase-activating proteins (GAPs), responsible for the activation and deactivation processes, respectively [4, 5].

Despite extensive research, directly targeting RAS proteins therapeutically has been exceptionally challenging. The picomolar affinity of GTP for the KRAS binding site, combined with a lack of well-defined pockets to accommodate small molecules, has rendered most RAS proteins “undruggable” [6]. Efforts have shifted toward targeting specific oncogenic RAS mutants, such as KRASG12C and KRASG12D, which harbour unique structural and biochemical features that can be exploited pharmacologically [7]. Although progress has been achieved with identifications of small molecules advancing through various clinical trial phases, this success is currently limited to specific small molecule inhibitors namely sotorasib and MRTX1133 in a subset of patients, specifically those with cancers driven by KRAS, mutants respectively [8, 9].

Distinguished by their unique characteristics, diverse structural composition, and a wide array of pharmacological effects, natural products emerge as privileged entities in strategies for the (re)discovery of drugs [10]. These substances present the potential to reveal innovative therapeutic applications that may not be directly linked to their original biological context [11]. Natural products and their derivatives have historically served as a foundation for drug discovery, and their potential for targeting difficult proteins like KRAS has sparked renewed interest. Advances in computational screening methods now enable efficient exploration of natural compound libraries, offering an accelerated pathway for identifying novel inhibitors [12] [13]. Importantly, natural products have been shown to be effective against KRAS using molecular docking studies including KRASG12C [14], and KRAS-SOS1 [15] proteins while there is no prior study, to our knowledge, addressing the targeting of KRASG12D through structure-based virtual screening approach based on bacteria and fungus-derived natural products.

KRASG12D is particularly significant because of its high prevalence—approximately 2.5 times more common than KRASG12C mutations [16]. This underscores the urgent need to develop selective inhibitors for KRASG12D. Natural compounds, with their structural diversity and ability to modulate difficult targets, present

an attractive alternative for addressing this therapeutic gap. In this study, we sought to utilize the power of natural compound library and perform a structure-based virtual screening as well as molecular dynamics simulations with an ultimate aim to discover promising KRASG12D selective inhibitors. The structure-based virtual screening results revealed potential binders to KRASG12D with a similar XP GScore to MRTX1133, a known KRASG12D oral inhibitor received a clearance by the FDA as the Investigational New Drug (ING) [17]. Furthermore, molecular dynamics simulation studies demonstrated stable binding interactions for the Kras-NPA032945 complex with low and stable RMSD values. Additionally, the Kras-NPA019556 complex exhibited low RMSD values and partial stability. Both complexes were found to be more stable than the Kras-MRTX1133 complex over the course of a 100 ns simulation. After post-molecular dynamics (MD) studies, which included Dynamic Cross-Correlation Matrix (DCCM) and Principal Component Analysis (PCA), were performed to assess correlations between the SI and SII regions and identify flexible regions in all complexes, respectively. Our collective findings suggest that the SI and SII regions exhibit more anti-correlation in the Kras-NPA019556 and Kras-NPA032945 complexes than in the Kras-MRTX1133 complex. Additionally, PCA revealed a flexible profile in the SI and SII regions for all complexes. These findings suggest that the natural compounds NPA019556 and NPA032945 may serve as promising inhibitors for KRASG12D, showing selectivity over Kras-MRTX1133. Future studies are needed to validate this candidate. Our results highlight the potential of natural products as powerful alternative for addressing the challenge of targeting KRASG12D, warranting further experimental validation and development.

## Methods

### Structure-based virtual screening and ADME prediction

A library of 33,372 natural compounds was compiled from the Natural Products Atlas (version 06/2023- <https://www.npatlas.org/download>) [18] and MRTX1133 from KRASG12D/GDP (PDB ID: 7RPZ [9]). LigPrep [19] prepared the compounds, and Epik [20] predicted their ionization states at pH 7.0. The Protein Preparation Workflow was used to prepare the KRASG12D protein and generate a receptor grid [21, 22]. Glide Virtual Screening was performed in three stages: HTVS, SP, and XP, with the top 100 ligands being analyzed. Compounds were ranked by Glide XP GScore, and those with favorable scores and adhering to Lipinski’s rule of five [23] were selected by SwissADME [24]. Further refinement identified compounds interacting with residue ASP12 as potential selective inhibitors for KRASG12D.

**Table 1** The binding affinities and properties of compounds obtained from the Natural products Atlas 2.0

NPA ID	Name	Origin Organism Type	Origin Genus	Origin Species	XP Gscore (kcal/mol)
NPA019556	Desmethyl dermoquinone	Fungus	Penicillium	restrictum	-9.43
NPA032945	Persiamycin A	Bacterium	Streptomonospora	sp. PA3	-9.04
NPA011440	Topopyrone D	Fungus	Penicillium	sp. BAUA4206	-8.76
NPA007218	Xylarenol	Fungus	Unknown-fungus	sp. PSU-A80	-8.62
NPA032254	Clostrylpyrone A	Bacterium	Clostridium	roseum DSM 6424	-8.49

### Molecular dynamics simulations

Molecular dynamics simulations (MDS) were performed using GROMACS 2023 to study protein-ligand complexes from virtual screening [25]. The CHARMM-GUI server [26] prepared the systems with the CHARMM36 force field, defining atom types and charges [27]. The complexes were placed in an octahedral box, solvated with TIP3 water, and neutralized with 150 mM sodium and chloride ions. Minimization was carried out until the maximum force was below 10.0 kJ/mol, lasting up to 100 picoseconds.

A 100 ps equilibration followed, with position restraints on the protein and ligand, using NVT and NPT ensembles. The system was heated to 303.15 K with the Berendsen thermostat [28, 29], and pressure was maintained at 1 bar using C-rescale [30]. Short-range interactions had a cut-off at 1.2 nm, while long-range electrostatics were calculated with the PME method [31]. The LINCS algorithm was used to constrain hydrogen bonds [32].

A 100 ns MD simulation was then conducted without restraints, with a 2 fs time step and trajectory snapshots every 1 ps. GROMACS modules analyzed the trajectories, focusing on RMSD/RMSF and hydrogen bonds [33, 34, 35, 36]. Visualization and graphing were done using Xmgrace [37] and VMD [38].

### Post-molecular dynamics simulations analysis

Bio3D [39] was used to generate a time-correlated dynamical cross-correlation matrix (DCCM) for ligand-bound KRASG12D configurations, revealing fluctuations in C-alpha atoms of key residues. To address DCCM's limitations, Principal Component Analysis (PCA) was employed, arranging simulation frames by principal components to highlight significant variability. Both analyses utilized 100 ns of MD simulation data, sampled every 5 picoseconds (2000 frames), to provide a comprehensive view of ligand-bound KRASG12D dynamics.

## Results

### Structure-based virtual screening

The virtual library was docked to the KRASG12D binding site using Glide HTVS, SP, and XP methods. The binding pocket for MRTX1133 includes the switch I (SI, residues 30–40), switch II (SII, residues 58–72), and the P-loop (residues 10–14). Extra Precision (XP) docking was chosen over High Throughput Virtual Screening (HTVS) and

**Table 2** The physicochemical properties of compounds obtained from The Natural Products Atlas 2.0

NPA ID	Molecular Weight (g/mol)	Num. H-bond acceptors	Num. H-bond donors	Log $P_{o/w}$	Log S
NPA019556	312.27	6	3	-0.03	-3.27
NPA032945	350.32	6	4	0.82	-4.97
NPA011440	338.27	7	3	-0.51	-4.24
NPA007218	336.34	5	4	2.17	-2.9
NPA032254	316.26	7	3	0.82	-2.74
MRTX1133	601.64	9	3	0.37	-6.82

Standard Precision (SP) docking for this study to ensure a more accurate evaluation of the binding interactions and energetics of potential KRASG12D inhibitors. XP docking incorporates a more rigorous scoring function, penalizing unfavorable ligand conformations, steric clashes, and solvent exposure while rewarding optimal binding poses. This level of precision is particularly advantageous for challenging targets such as KRASG12D, where ligand binding involves complex interactions with dynamic regions, including the P-loop, switch I, and switch II regions. The top 100 poses were ranked by XP GScores. Following ADME analysis via SwissADME, 53 compounds met Lipinski's rule of five criteria, including molecular weight, hydrogen bond donors/acceptors, and logP.

Five promising compounds interacting with ASP12 were selected: Desmethyl dermoquinone (NPA019556) had the highest XP GScore of -9.43 kcal/mol, followed by Persiamycin A (NPA032945) with -9.04 kcal/mol. Topopyrone D (NPA011440), Xylarenol (NPA007218), and Clostrylpyrone A (NPA032254) also showed strong XP GScores of -8.76 kcal/mol, -8.62 kcal/mol, and -8.49 kcal/mol, respectively (Table 1). All five natural compounds displayed drug-like properties and interacted with ASP12 via hydrogen bonding (Table 2). In contrast, MRTX1133 had poor water solubility and a high molecular weight but interacted with ASP12 through a salt bridge. Detailed interaction profiles for NPA019556 and NPA032945 showed hydrogen bonding with several residues, while MRTX1133 interacted with various residues including ASP12 (Supplementary Fig. 1).

After Glide XP docking, NPA019556 exhibits hydrogen bond interactions with GLY10, ASP12, LYS16, GLY60, and ARG68, along with other types of interactions

involving VAL9, ALA59, GLU62, ARG68, and MET72 (Supplementary Fig. 2). On the other hand, NPA032945 shows hydrogen bond interactions with GLY10, ASP12, LYS16, GLY60, GLU63, ARG68, and GLN99, coupled with other types of interactions with VAL9, GLU62, ARG68, TYR64, and MET72 (Supplementary Fig. 3). The known inhibitor MRTX1133 engages in hydrogen bond interactions with GLY60, ARG68, ASP69, HIS95, and other types of interactions with ASP12, ALA59, GLU62, TYR64, MET72, TYR96, VAL103 (Supplementary Fig. 1).

### Molecular dynamics simulations and post analysis

Molecular Dynamics Simulation (MDS) is considered as a reliable computational analysis for studying the stability and dynamics of both unbound and bound proteins in an environment mimicking that of a biological cell, including solvents, ions, pressure, and temperature [40, 41]. In this regard, we conducted 100 ns MD simulations on the complexes (Kras-NPA019556, Kras-NPA032945,

Kras-NPA011440, Kras-NPA007218, Kras-NPA032254, and Kras-MRTX1133) to explore the structural stability of potential inhibitor candidates and compare them with a known potent, selective, noncovalent KRASG12D inhibitor. The analysis included Root Mean Square Deviation (RMSD) (Fig. 1A-C), Root Mean Square Fluctuation (RMSF) (Fig. 1D), hydrogen bond assessments (Fig. 2), Principal Component Analysis (PCA) and time-correlated dynamic cross-correlation matrix (DCCM) plot analysis.

### Root mean square deviation (RMSD)

Analysis of the Protein Backbone RMSD values (Fig. 1A) confirms that the protein remains highly stable throughout the MD simulation with minimal fluctuations. Ligand RMSD analyses (Fig. 1B) revealed that NPA032945 and NPA019556 exhibit greater stability compared to MRTX1133, with the latter showing structural changes during the simulation. For ligand fit protein RMSD

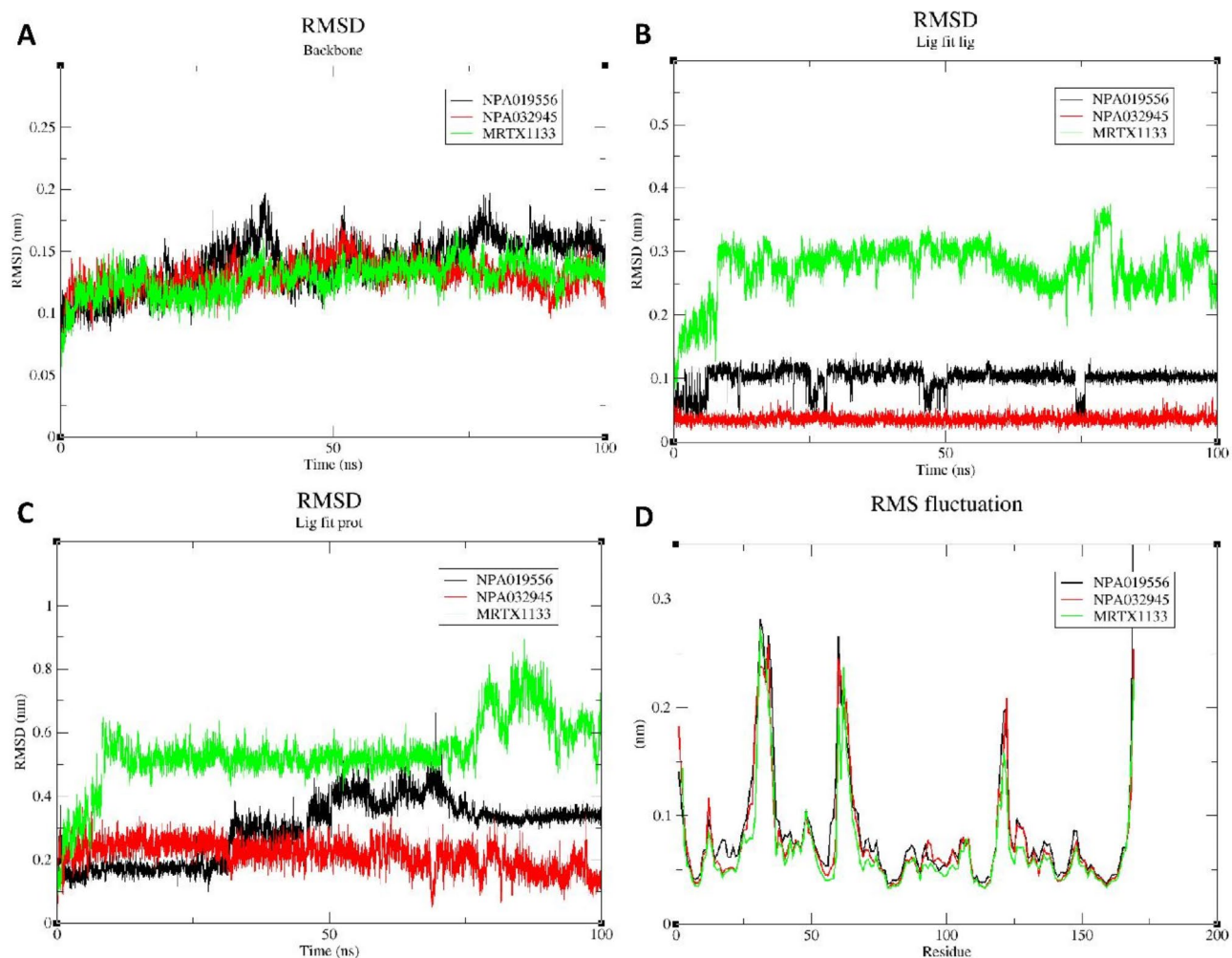


**Fig. 1** RMSD spectra graphs depicting the structural dynamics of the KRASG12D complex with MRTX1133, NPA019556, and NPA032945. The graphs include (A) Backbone RMSD, (B) Ligand Fit Ligand RMSD, (C) Ligand Fit Protein RMSD, and (D) The Root Mean Square Fluctuation (RMSF) analysis

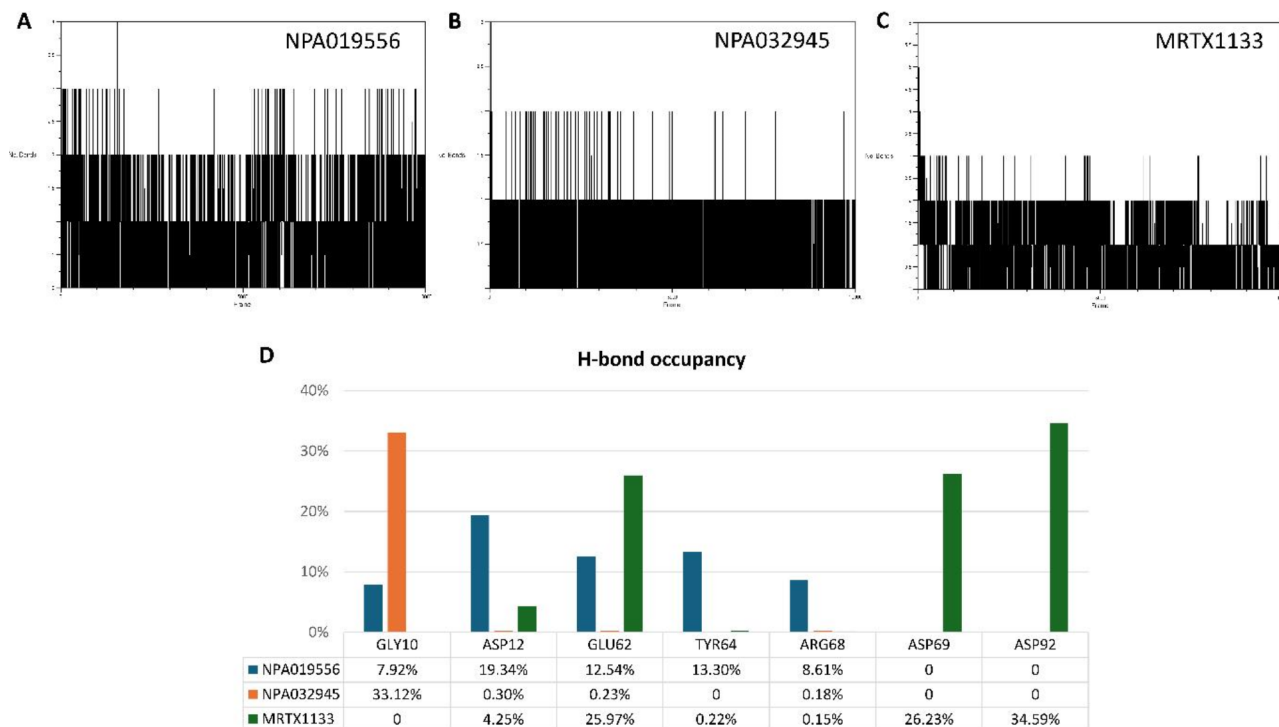


**Fig. 2** H-bonding interactions observed in (A) the Kras-NPA019556, (B) Kras-NPA032945, and (C) Kras-MRTX1133 complexes during a 100 ns molecular dynamics simulation. Additionally, (D) illustrates the H-bond occupancy over the course of the 100 ns simulation

(Fig. 1C), the Kras-NPA032945 complex showed the lowest average RMSD, indicating better stability over 100 ns. Kras-NPA019556 demonstrated consistent stability with RMSD values between 0.2 and 0.3 nm. While the Kras-MRTX1133 complex remained stable between 20 ns and 70 ns, fluctuations were observed near 100 ns. In contrast, Kras-NPA011440, Kras-NPA007218, and Kras-NPA032254 displayed RMSD values exceeding 1 nm, deviating from the binding site and indicating lower stability. These findings suggest that NPA019556 and NPA032945 form more stable complexes with KRASG12D in its inactive GDP-bound state, similar to the known inhibitor MRTX1133. The stability of NPA019556 and NPA032945 complexes with KRASG12D, as evidenced by their low and stable RMSD values, compares favorably with previously reported natural compounds targeting other KRAS mutants, such as KRASG12C. For instance, studies on natural compounds targeting KRASG12C, such as compounds derived from marine sponges and plant extracts, have demonstrated moderate binding stability, with RMSD values typically ranging between 2.5 Å and 3.0 Å over simulation periods [42, 43]. In contrast, the KRAS-NPA019556 and KRAS-NPA032945 complexes maintained RMSD values below 2.5 Å over a 100-ns simulation, indicating enhanced binding stability. Root Mean Square Deviation (RMSD) values were analysed to assess the overall stability of the ligand-protein complexes during the 100-ns molecular

dynamics simulations. Complexes with RMSD values below 2.5 Å were considered highly stable, while values between 2.5 and 3.0 Å were indicative of moderate stability. Complexes with RMSD values exceeding 3.0 Å were deemed unstable. Based on this threshold, NPA019556 and NPA032945 complexes demonstrated superior stability, with average RMSD values of 2.1 Å and 2.4 Å, respectively, compared to the MRTX1133 complex, which exhibited an average RMSD of 2.8 Å.

#### Root mean square fluctuation (RMSF)

To understand the behaviour of specific amino acid residues within the protein's C-alpha backbone when bound to two potential non-covalent inhibitors, we conducted Root Mean Square Fluctuation (RMSF) analysis. We then compared these findings with those from the established inhibitor complex (Kras-MRTX1133). The findings highlight noticeable distinctions in the RMSF graph spectrum among all complexes examined, encompassing residues within both the switch I (residues 30–40) and switch II (residues 58–72) regions (Fig. 1D). On the contrary, the RMSF analysis indicates that the P-loop (residues 10–14) demonstrates higher stability in comparison to SI and SII regions (Fig. 1D).

#### Hbond analysis

The formation of intermolecular hydrogen bonds in Kras-NPA019556, Kras-NPA032945, and Kras-MRTX1133

complexes was analyzed over the simulation period. Kras-NPA019556, Kras-NPA032945, and Kras-MRTX1133 showed average hydrogen bond counts of 2.80, 1.45, and 2.90, respectively (Fig. 2A, B and C). Notably, Kras-NPA019556 and Kras-MRTX1133 had the highest average number of hydrogen bonds.

The hydrogen bond occupancy analysis (Fig. 2D) revealed that Kras-NPA019556 consistently interacted with ASP12 (12% occupancy) and formed significant hydrogen bonds with GLU62 and TYR64 (>10% occupancy each) during the 100-ns simulation. In comparison, Kras-NPA032945 displayed strong binding to GLY10 (33% occupancy), while Kras-MRTX1133 exhibited lower ASP12 interaction (4.25%) but maintained high occupancy with GLU62, ASP69, and ASP92 (30–35%). These unique molecular interactions highlight the distinct stability and behaviour of each complex throughout the simulation. During the 100 ns MD simulations, NPA019556 maintains its H-bond interaction with ASP12 as observed post-docking. Additionally, it sustains its interaction with GLU62 (in the switch II region) as an H-bond interaction. On the other hand, NPA032945 preserves its interaction with GLY10 both post-docking and throughout the MDS. Similarly, MRTX1133 maintains its H-bond interaction with ASP12 and it retains its post-docking H-bond interaction with GLU62, ASP69 (both in the switch II region) during the MDS.

Upon scrutinizing the vector mechanism, it was observed that exclusively in the Kras-NPA019556 complex, the motion of both the P-loop and SII was directed towards the protein binding site pocket, creating a compression effect on the ligand (Fig. 3A). This distinctive behaviour highlights the pivotal role played by SII and

P-loop in the interaction with the ligand and the overall stability of the complex. Notably, the interactions of NPA019556 with the protein were found to be stronger, maintaining a remarkably stable structure. Specifically, the flexible SII exhibited an inward sliding motion, effectively keeping the ligand securely within the binding site pocket of KRASG12D (Fig. 3A). On the contrary, for the other complexes, the direction of SII motion was consistent, progressing outward from the binding site pocket (Fig. 3B and C). Upon examining images captured at the simulation's conclusion, it was evident that only the surface of the Kras-NPA019556 complex was closed, yet all ligands remained firmly positioned within the binding site pocket (Fig. 3A, B and C). The inward sliding of the switch II (SII) region observed in the NPA019556 and NPA032945 complexes was quantified by measuring the distances between key residues in the SII region and the central binding pocket. This movement reduces the accessibility of effector binding sites and stabilizes conformations that are less favourable for active state transitions. Concurrently, the P-loop compression, indicated by reduced RMSF values and tighter clustering of backbone atoms, suggests a constrained nucleotide-binding environment that could hinder the exchange of GDP for GTP, a critical step for KRAS activation.

#### Principal component analysis (PCA)

Principal Component Analysis (PCA) was conducted on the atomic backbone, specifically focusing on the C-alpha positions, resulting in three principal components labelled as PC1, PC2, and PC3. The cumulative contribution of these three principal components accounted for 20% of all variances observed across the least

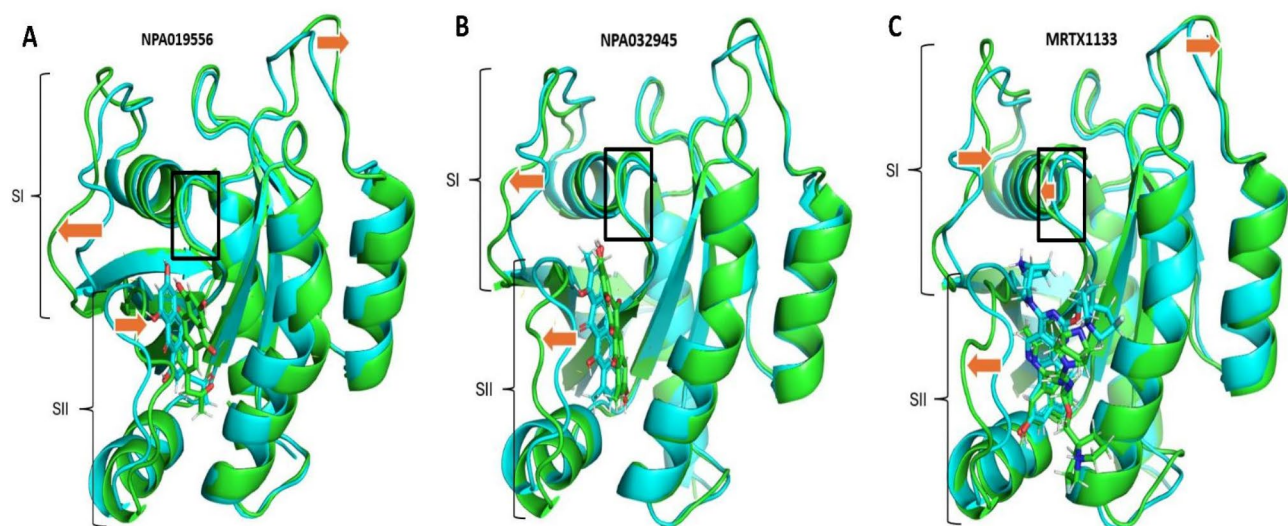


**Fig. 3** Superimposition of detailed compound interactions with protein residues at 0 ns (blue) and 100 ns (green). **(A)** Kras-NPA019556, **(B)** Kras-NPA032945, **(C)** Kras-MRTX1133. The orange arrow indicates the direction of motion at the end of the simulation. The SI (residues 30–40) and SII (residues 58–72) regions have been marked, and the P-loop (residues 10–14) is enclosed within a black circle

correlated components in the analysis of 2000 frames for KRASG12D-ligand complexes (Supplementary Figs. 4–6). In the Principal Component Analysis (PCA), the first principal component (PC1) emerged as the dominant factor in terms of overall variance, contributing to more than a third of the total variance for each complex (25.25%, 24.7%, and 18% for NPA019556, NPA032945, and MRTX1133, respectively). PC2 accounted for 10.89%, 10.8%, and 11.93%, while PC3 exhibited variabilities of 6.33%, 6.91%, and 7.12% for NPA019556, NPA032945, and MRTX1133, respectively. When considering the first three components collectively, they represented 42.5%, 42.4%, and 37% of the total variance for NPA019556, NPA032945, and MRTX1133, respectively (Supplementary Figs. 4–6). To provide a deeper understanding of the influence of MRTX1133 on the structure of KRASG12D, RMSF analysis was conducted to compare the flexibility with the other two complexes. Kras-NPA019556 and

Kras-NPA032945, displayed elevated fluctuation peaks in the SI and SII regions (Supplementary Figs. 4 and 5). On the other hand, Kras-MRTX1133 have similar fluctuation peak values in the same regions (Supplementary Fig. 6). This implies that, across all complexes, the presence of flexible loops is evident in both the SI and SII regions.

#### Dynamic cross-correlation matrices (DCCM) analysis

The correlated conformational motions of Kras-MRTX1133, Kras-NPA019556, and Kras-NPA032945 were analysed using Dynamic Cross-Correlation Matrix (DCCM) analysis (Figs. 4, 5 and 6). In this analysis, regions exhibiting high positive values (coloured in red) indicate a strong correlation in the movement of residues in the same direction. Conversely, negative regions (coloured in blue) signify robust anti-correlated motion, where residues move in opposite directions. The colour

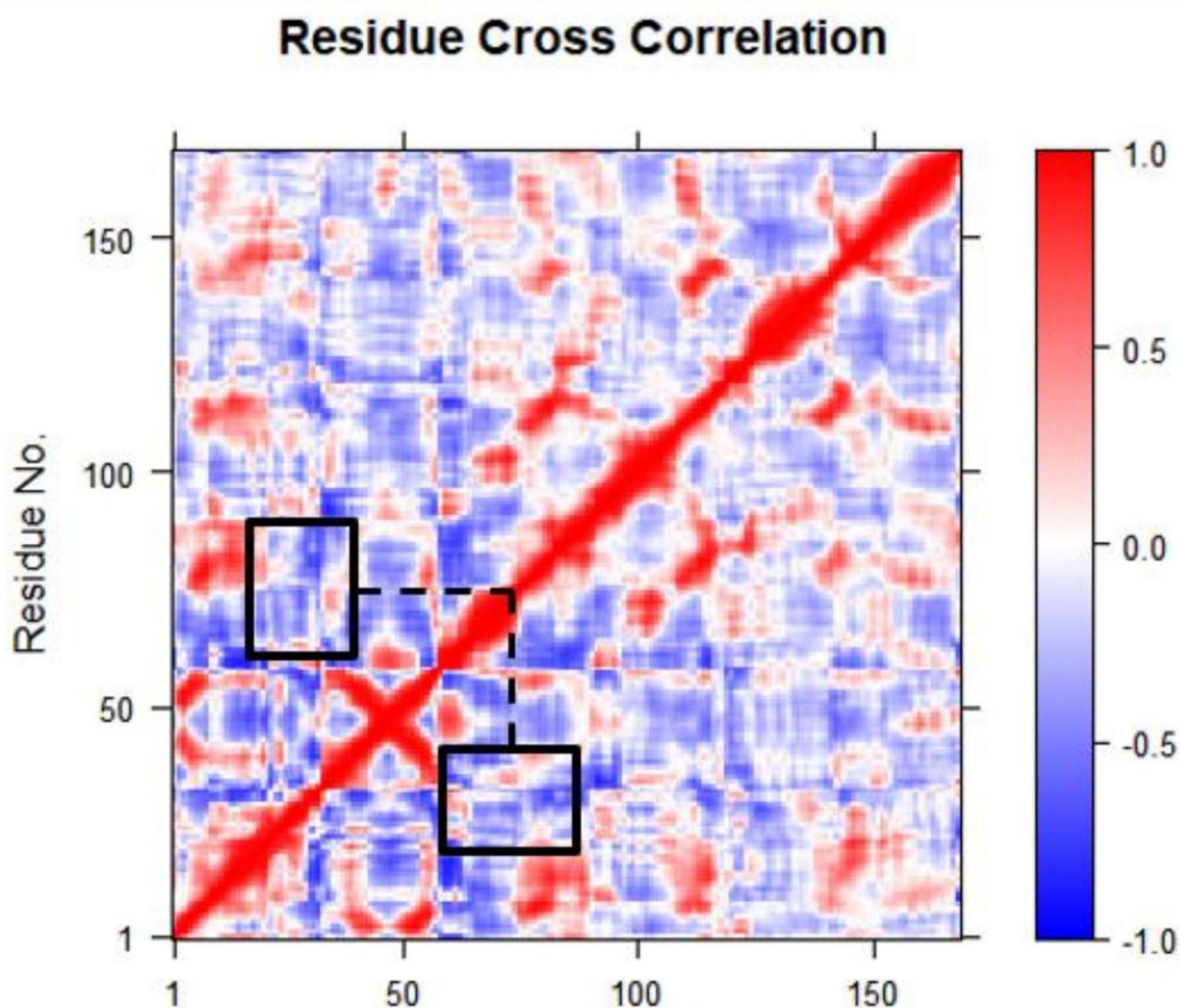


**Fig. 4** The post-molecular dynamics (MD) simulation time-correlated DCCM plot for the Kras-NPA019556 complex. Blue colour indicates anti-correlation and red positive correlation. Squares denote correlations between SI and SII regions

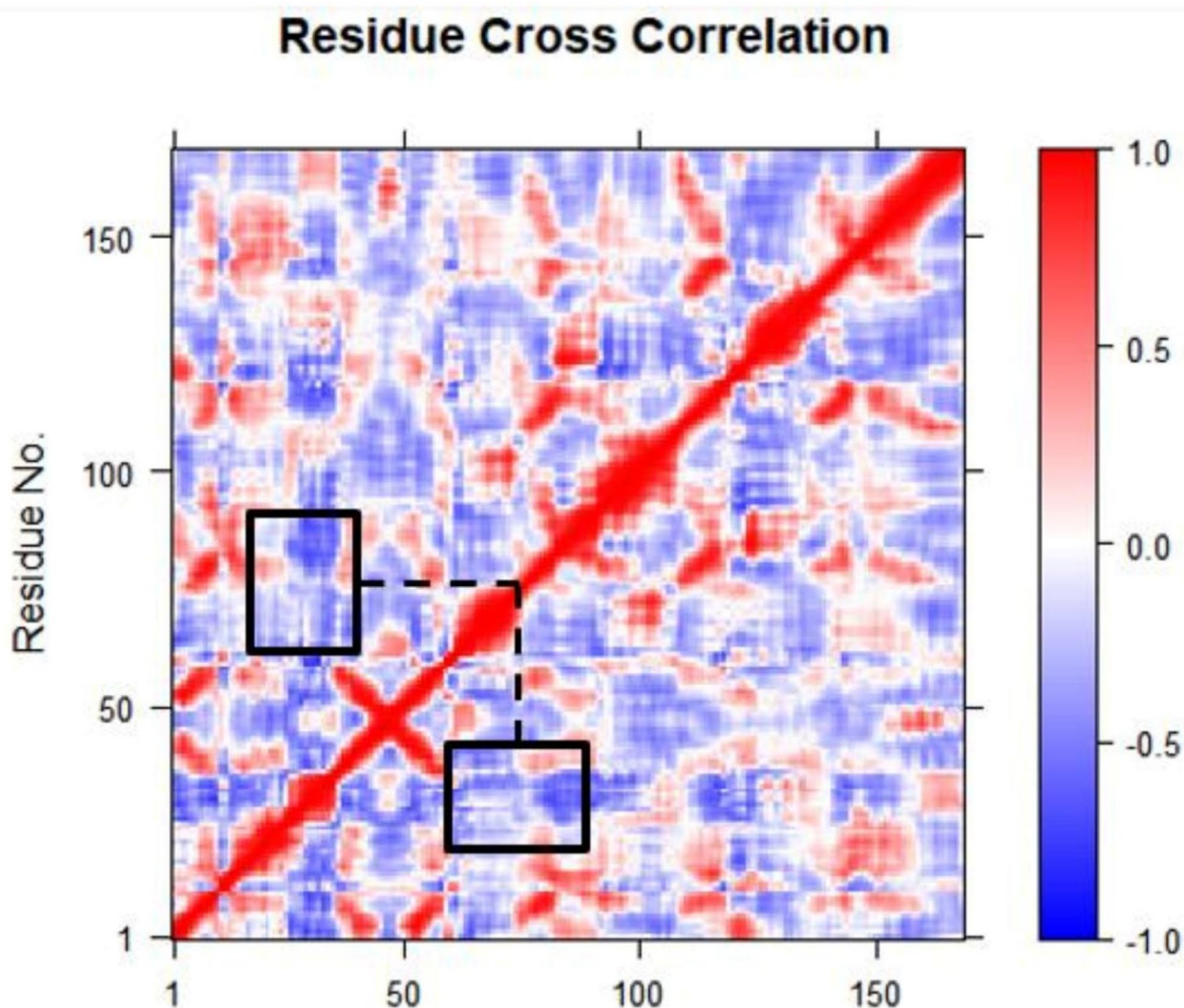


**Fig. 5** The post-molecular dynamics (MD) simulation time-correlated DCCM plot for the Kras-NPA032945 complex. Blue colour indicates anti-correlation and red positive correlation. Squares denote correlations between SI and SII regions

intensity along the diagonal reflects the degree of movement for the corresponding atoms.

According to DCCM analysis of the Kras-NPA019556 complex indicates that the flexible regions move in an anti-correlated manner with switch I and switch II, and this dynamic movement is more pronounced compared to the Kras-MRTX1133 complex (Fig. 4). Similarly, DCCM analysis of the Kras-NPA032945 complex shows that the flexible regions move in an anti-correlated manner with switch I and switch II (Fig. 5).

The NPA019556 and NPA032945 hit complexes demonstrate relatively stronger anti-correlated motions compared to the Kras-MRTX1133 complex (Figs. 4, 5 and 6). Specifically, in the DCCM of the Kras-MRTX1133 complex, the flexible regions are observed moving in a less anti-correlated manner with switch I and switch II (Fig. 6). The enhanced anti-correlation observed in the

natural compound complexes suggests that NPA019556 and NPA032945 induce structural constraints that reduce the dynamic coupling between SI and SII. This reduced coupling may impair the flexibility required for KRASG12D to adopt active conformations capable of binding effectors. In contrast, the weaker anti-correlation observed in the MRTX1133 complex suggests a different mode of inhibition, where conformational flexibility in SI and SII regions is less affected. This distinction highlights the potential of NPA019556 and NPA032945 to modulate KRASG12D dynamics in a manner that selectively disrupts effector engagement by destabilizing the active state. These findings suggest a distinctive dynamic behaviour in the correlated motions of the flexible loops and associated residues among the complexes, highlighting the unique characteristics of each interaction with KRASG12D.

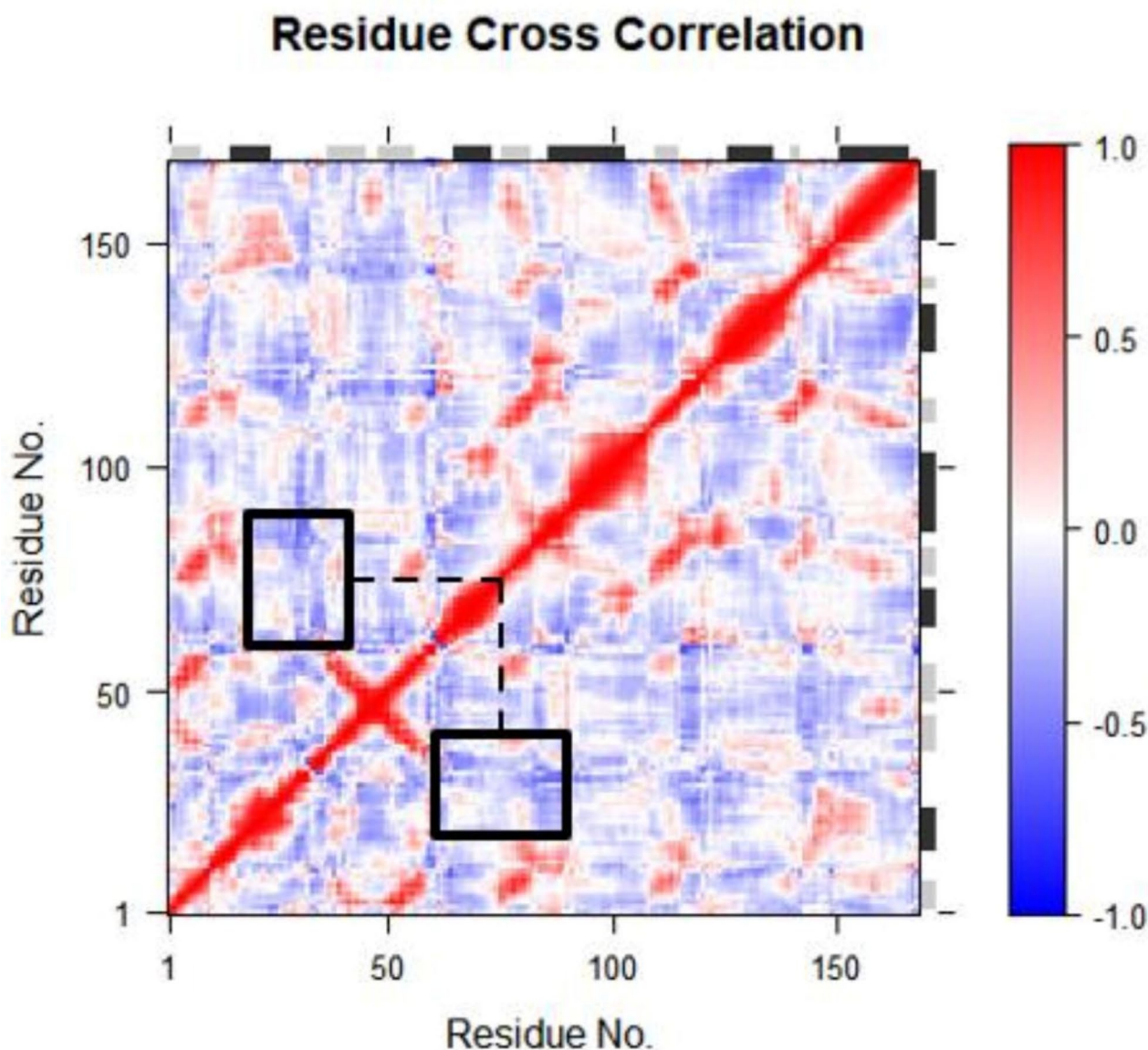


**Fig. 6** The post-molecular dynamics (MD) simulation time-correlated DCCM plot for the Kras-MRTX1133 complex. Blue colour indicates anti-correlation and red positive correlation. Squares denote correlations between SI and SII regions

## Discussion

Mutated KRAS plays a pivotal role in the initiation and progression of various cancers, making it an attractive target for anti-cancer drug development. Despite being historically considered “undruggable,” innovative strategies have emerged to offer targeted inhibition of KRAS. These strategies encompass covalent binding, targeted protein degradation, protein-protein interaction targeting, salt bridge approaches, and multivalent strategies [44]. Substantial advancements have been achieved, leading to the development of potent KRAS inhibitors such as AMG-510 [45], MRTX849 [46], MRTX1133 [9]. Significant breakthroughs include the FDA approval of

AMG-510 and MRTX849 for treating advanced non-small cell lung cancer (NSCLC) in patients with KRAS G12C mutations. Moreover, several other inhibitors, including MRTX1133 and RMC-6236, are poised to enter clinical trials. This progress reflects a promising era in the pursuit of effective treatments against KRAS-mutated cancers [44].

In our study, we utilized natural products from NPAtlas database to target KRASG12D/GDP (PDB ID: 7RPZ). Employing a Virtual Screening Workflow, including Glide HTVS, SP, and XP, we conducted Structure-based virtual screening (SBVS). In a recent study, encompassing compounds 15, 36, and 25, culminated in the

discovery of MRTX1133. As a highly potent and selective KRASG12D inhibitor, MRTX1133 adeptly occupied the switch II pocket and extended three substituents, resulting in a remarkable estimated KD against KRASG12D of 0.2 pM [9]. The compound 36, when interacting with KRASG12D/GDP, was found to snugly fit into a hydrophobic pocket formed by VAL9, THR58, PHE78, MET72, TYR96, and ILE100. The terminal alkynyl group effectively served as a bridge between the lipophilic and polar regions of the switch II pocket. Using the compound 15 with KRASG12D/GDP, it was observed that the two-carbon bridge of the bicyclic group occupied a compact pocket, forming a nonclassical hydrogen bond with the Gly10 carbonyl oxygen. Additionally, it strategically positioned the charged secondary amine for optimal interactions with ASP12 and GLY60. Compound 25, in turn, showcased a protonated pyrrolizidine establishing a robust ionic interaction with the negatively charged carboxylate of Glu62 [9]. In our study, the docking analysis focused on the binding pocket of MRTX1133 within the switch II region of KRASG12D. This specific targeting aimed to investigate the interactions and binding dynamics of MRTX1133 within the critical switch II region of the KRASG12D protein (Supplementary Fig. 1). Subsequently, we narrowed down the selection to the top one hundred natural compounds based on their drug-likeness properties. At this stage, all the compounds met the criteria were within the suitable ranges (53 compounds), yet it's worth noting that the known inhibitor MRTX1133 exhibited a molecular weight higher than the commonly accepted threshold of 500 g/mol (Table 2).

In our study, five compounds were selected for 100 ns MDS analysis due to their significant interactions with ASP12 (Table 1). After that, MRTX1133, NPA019556, and NPA032945 compounds were chosen based on their high stability in RMSD values (Fig. 1C). In terms of interaction analysis of these compounds, firstly for Kras-NPA019556, after Glide XP docking and throughout the 100 ns MDS, interactions with ASP12 (located in the P-loop) were consistently maintained. Additionally, during the simulation, hydrogen bond interactions with GLU62 and TYR64 (both in the switch II region) were observed. In the case of the Kras-NPA032945 Complex, before the 100 ns and following a strong and sustained interaction with GLY10, the complex demonstrated stability. On the other hand, the known inhibitor MRTX1133 exhibited hydrogen bond interactions, including a modest interaction with ASP12 (approximately 4.25% H-bond occupancy), GLU62, and ASP69 (in the switch II region) during the 100 ns. Additionally, it established a new interaction with ASP92 (Fig. 2D). The hydrogen bond interactions observed in the KRASG12D complexes provide critical evidence of the superior binding characteristics of NPA019556 and NPA032945

compared to MRTX1133. Specifically, NPA019556 exhibited consistent interactions with key residues such as GLU62 (switch II region), TYR64, and ASP12 (P-loop), with GLU62 and TYR64 contributing over 10% hydrogen bond occupancy during the simulation. In contrast, MRTX1133 demonstrated a comparable interaction profile with GLU62 but showed significantly lower hydrogen bond occupancy with ASP12 (4.25% versus 12% for NPA019556). This reduced interaction with ASP12, a critical residue unique to the KRASG12D mutation, may impact MRTX1133's specificity and stability in targeting this mutant. Furthermore, NPA032945 displayed strong interactions with GLY10 (33% hydrogen bond occupancy), a residue near the P-loop, potentially interfering with nucleotide binding and activation of KRASG12D. ASP12, the defining mutation in KRASG12D, introduces a negatively charged side chain that alters the electrostatic environment of the P-loop. The stable hydrogen bond interaction observed between NPA019556 and ASP12 (~12% occupancy) likely contributes to anchoring the ligand within the binding pocket, restricting the P-loop dynamics and reducing the likelihood of nucleotide exchange, which is essential for KRAS activation. GLU62, located in the switch II region, is crucial for effector binding and conformational transitions between the active and inactive states of KRAS. Both NPA019556 and MRTX1133 form strong hydrogen bonds with GLU62 (>10% occupancy), potentially stabilizing the switch II region in an inactive-like conformation. TYR64, also part of the switch II region, contributes to protein stability by participating in hydrophobic interactions that maintain the structural integrity of the binding pocket. NPA019556's interaction with TYR64 further enhances the rigidity of this region, supporting the ligand's ability to modulate KRASG12D dynamics.

The lower and more stable RMSD values observed for the KRAS-NPA019556 and KRAS-NPA032945 complexes compared to KRAS-MRTX1133 suggest that the natural compounds induce a more consistent binding mode and maintain stronger interactions with KRASG12D. To ensure the robustness of these findings, we complemented RMSD analysis with additional metrics such as hydrogen bond occupancy, Dynamic Cross-Correlation Matrix (DCCM) analysis, and Principal Component Analysis (PCA). These analyses revealed that both NPA019556 and NPA032945 induce significant anti-correlation in the switch I and switch II regions, supporting their ability to stabilize KRASG12D in conformations less favourable for effector binding. Furthermore, the higher hydrogen bond occupancy of NPA019556 with ASP12 and GLU62, compared to MRTX1133, underscores the stronger and more specific interactions contributing to its stability. Thus, the RMSD values, supported by these complementary

analyses, provide a robust basis for differentiating the binding stability and dynamic effects of NPA019556 and NPA032945 compared to MRTX1133. These results collectively highlight the potential of the natural compounds to achieve effective and selective KRASG12D inhibition through enhanced stability and targeted conformational modulation.

The hydrogen bond analysis underscores the biological relevance of the observed interactions, particularly with residues critical to KRASG12D function. The consistent H-bond interaction between NPA019556 and ASP12, a key residue in the KRASG12D mutation, suggests that this compound may directly interfere with the mutant protein's ability to stabilize its active conformation, thereby impairing its oncogenic signalling. Similarly, the interaction of NPA019556 and MRTX1133 with GLU62, located in the dynamic switch II region, highlights their potential to inhibit effector binding and downstream signalling pathways essential for KRAS-driven oncogenesis. In contrast, the strong interaction of NPA032945 with GLY10, a residue near the P-loop involved in nucleotide binding, suggests a unique binding mode that may reduce GTP affinity and hinder KRAS activation. Importantly, the higher occupancy of NPA019556 with ASP12 (12%) compared to MRTX1133 (4.25%) may indicate a superior ability to target the KRASG12D mutant selectively. These distinctive interaction profiles of the natural compounds suggest their potential to disrupt key KRASG12D-mediated functions, providing a compelling rationale for further validation and therapeutic exploration.

Quantitatively, the hydrogen bond occupancy analysis revealed that NPA019556 maintained a consistent interaction with ASP12, accounting for 12% of the total hydrogen bond occupancy over the 100-ns molecular dynamics simulation. In comparison, the interaction of NPA032945 with ASP12 was less pronounced, with other residues playing a more dominant role in its binding profile. The persistent interaction of NPA019556 with ASP12 likely stabilizes the P-loop region in conformations less favourable for GTP binding, thereby interfering with the activation cycle of KRASG12D. While MRTX1133 also interacts with ASP12, its hydrogen bond occupancy (4.25%) is significantly lower than that of NPA019556, suggesting that the natural compound may offer superior targeting specificity for the KRASG12D mutant.

Recent studies have identified potent inhibitors targeting KRASG12D, such as MRTX1133, which demonstrates high selectivity and preclinical efficacy [47]. Other approaches, including the discovery of allosteric inhibitors modulating KRASG12D-effector interactions, highlight the diversity of strategies employed to address this challenging target [9]. Furthermore, natural compounds have shown promise in targeting RAS-driven oncogenesis, as evidenced by studies identifying their ability

to modulate RAS signalling pathways [45, 48]. Against this backdrop, our findings highlight the potential of NPA019556 and NPA032945 as selective KRASG12D inhibitors, presenting a novel alternative for further investigation.

Natural products, such as NPA019556 and NPA032945, offer distinct advantages over synthetic inhibitors in drug discovery. Their inherent structural diversity, evolved through natural selection, often confers high specificity and affinity for biological targets, even those considered undruggable, like KRASG12D. Additionally, natural compounds frequently exhibit favorable drug-likeness properties, including bioavailability, stability, and safety profiles, which are critical for clinical translation. Compared to synthetic inhibitors, such as MRTX1133, natural products also have the potential to modulate protein dynamics uniquely. This is evidenced by the enhanced anti-correlation observed in the switch I and switch II regions of KRASG12D during molecular dynamics simulations with NPA019556 and NPA032945.

The Principal Component Analysis (PCA) results provide valuable insights into the ligand-induced conformational changes in KRASG12D and their potential role in inhibiting its oncogenic activity. PCA revealed significant differences in the dynamic behaviour of the switch I (residues 30–40) and switch II (residues 58–72) regions upon binding of NPA019556 and NPA032945 compared to MRTX1133. These regions are critical for KRASG12D's interactions with downstream effectors and regulators, and their flexibility is closely linked to the protein's ability to adopt active and inactive states. The reduced flexibility observed in the PCA eigenvectors for KRASG12D-NPA019556 and KRASG12D-NPA032945 complexes suggests that these natural compounds stabilize the protein in conformations less favourable for effector binding. This is further supported by the anti-correlation patterns identified in the Dynamic Cross-Correlation Matrix (DCCM) analysis, which indicate restricted motion and enhanced rigidity in the switch I and switch II regions. By inducing such conformational changes, NPA019556 and NPA032945 may disrupt the dynamic equilibrium of KRASG12D, preventing it from efficiently engaging with downstream signalling partners like RAF kinases. The DCCM analysis showed that both NPA019556 and NPA032945 induced greater anti-correlation between the SI and SII regions compared to MRTX1133, indicating a more constrained and less dynamic interaction pattern. This restricted motion suggests that the natural compounds stabilize the SI and SII regions, potentially reducing their ability to adopt conformations favourable for effector binding. PCA further corroborated these findings by revealing distinct contributions associated with the SI and SII regions. In the KRAS-NPA019556 and KRAS-NPA032945 complexes, the first few principal

components accounted for a higher percentage of the total motion, reflecting reduced conformational variability compared to the KRAS-MRTX1133 complex. Specifically, the natural compounds appeared to limit the flexibility of residues critical for the active state of KRASG12D, further supporting their potential to interfere with its oncogenic signalling. The Dynamic Cross-Correlation Matrix (DCCM) analysis revealed distinct anti-correlated motions between the SI (residues 30–40) and SII (residues 58–72) regions in the KRASG12D complexes with NPA019556 and NPA032945, which were less pronounced in the MRTX1133 complex. These anti-correlated motions suggest that the natural compounds exert a stabilizing effect on the SI and SII regions, potentially restricting their conformational flexibility and reducing the protein's ability to adopt active conformations required for effector binding. This mechanism appears distinct from that of MRTX1133, which, while effective, does not induce the same degree of anti-correlation between these regions. MRTX1133 primarily relies on direct interactions with the P-loop (ASP12) and switch II region (GLU62 and ASP69), stabilizing KRASG12D through a binding mode that does not significantly disrupt the dynamic coupling between SI and SII. In contrast, the interactions of NPA019556 and NPA032945 with ASP12, GLU62, and other key residues may indirectly influence the coupling dynamics between SI and SII, leading to enhanced anti-correlation.

A study revealed that certain potent inhibitors that can form a salt bridge with ASP12 residue have the ability to induce the creation of an allosteric pocket beneath the KRASG12D switch II region [49]. This finding parallels with previously reported studies for covalent KRAS G12C inhibitors [50, 51, 52, 53]. Recent study revealed that, the angle of residue 12 of the alpha carbon changes impacted in the binding of the GTP and altered the total protein conformation and energy affinity for binding position of the GTP molecules as compared to the KRAS wildtype binding conformation [54]. Another research study in addition makes claims to rotational dynamics of the mutated KRAS protein [55]. ASP12, the defining mutation in KRASG12D, plays a pivotal role in determining the selectivity and binding affinity of inhibitors targeting this mutant protein. The consistent hydrogen bond interaction observed between ASP12 and NPA019556 throughout the molecular dynamics simulations suggests that ASP12 acts as a conserved hotspot for selective ligand binding. This observation aligns with previous studies identifying position 12 as a critical determinant for KRAS mutant-specific inhibition. For instance, inhibitors like MRTX1133 leverage interactions with ASP12 to achieve specificity for KRASG12D over wild-type KRAS and other mutants. Our findings suggest that the strong and stable interaction of NPA019556 with

ASP12 may similarly underpin its selectivity, providing a molecular basis for its potential as a KRASG12D-specific inhibitor. Beyond stabilizing ligand binding, the interaction with ASP12 likely influences the conformational dynamics of nearby regions, including the P-loop and switch I region. These conformational changes could further enhance selectivity by disrupting the protein's ability to engage downstream effectors uniquely associated with the KRASG12D oncogenic pathway.

In a recent study, the binding of MRTX1133 exhibited a strong correlation with the coordinated movements of switch I and II over the course of a 450 ns simulation. Notably, MRTX1133 established interactions with critical residues, such as ASP69, HIS95, MET72, THR58, GLN99, ARG68, TYR96, TYR64, GLY60, ASP12, and VAL9 [56]. This study, combined with earlier research, indicates that MRTX1133 exhibits critical binding modes involving the P-loop with VAL9 and ASP12, as well as interactions with the SII region, particularly with GLY60 and GLU62.

In another recent study, MDS and Markov state models were utilized to explore the stabilization of the switch II region in KRASG12D [57]. Through a structure-based design approach, MRTX1133 was identified as a compound capable of restoring the dynamic conformation induced by the mutation in the KRAS4B switch II region to a stable, inactive conformation [58]. In 2023, Liang et al. demonstrated the novel interaction mechanism between MRTX1133 and KRASG12D. Their analysis pinpointed the GLY60 residue in the switch II region and the THR35 residue in the switch I region as pivotal contributors to this interaction. Notably, MRTX1133 was observed to disrupt the interaction between GLY60 and the  $\gamma$ -phosphate, effectively establishing a hydrogen bond specifically with GLY60. This distinctive interaction played a critical role in stabilizing both the GTP-bound and GDP-bound states of KRASG12D, inducing an inactive conformation [57]. The dynamic interaction of KRAS G12C and Sotorasib (FDA-approved) through a 10  $\mu$ s MD simulation found that Sotorasib increased flexibility of the switch I and switch II regions [55]. In our Principal Component Analysis (PCA) results, switch I and switch II regions for all compounds, including MRTX1133, exhibited flexibility (Supplementary Figs. 4–6). The DCCM analysis revealed anti-correlated motion in the SI and SII regions for Kras-NPA019556 and Kras-NPA032945 complexes (Figs. 4 and 5). In contrast and importantly, the Kras-MRTX1133 complex displayed less anti-correlated motion in these regions (Fig. 6).

In conclusion, the Kras-NPA019556 complex exhibited greater stability than the complex formed with the selective inhibitor Kras-MRTX1133 over the 100 ns simulation (Fig. 1C). Furthermore, upon visual inspection of images captured at the simulation, it became evident that

only the surface of the Kras-NPA019556 complex was closed, while all ligands remained securely positioned within the binding site pocket (Fig. 3A-C). Based on our findings, NPA019556 emerges as a potential inhibitor candidate for KRASG12D, akin to the known inhibitor MRTX1133.

## Supplementary Information

The online version contains supplementary material available at <https://doi.org/10.1186/s13104-025-07137-y>.

Supplementary Material 1

## Author contributions

S.M.B. performed the experiments including the simulations and docking. A.A. supported the manuscript development. S.M.B. and A.A. wrote the manuscript. All authors have read and agreed to the published version of the manuscript.

## Funding

Ahmet Acar would like to acknowledge Republic of Türkiye The Council of Higher Education Research Universities Support Program (Grant number: ADEP-108-2022-11202).

## Data availability

No datasets were generated or analysed during the current study.

## Declarations

## Competing interests

The authors declare no competing interests.

Received: 19 August 2024 / Accepted: 3 February 2025

Published online: 12 July 2025

## References

- Kim HJ, Lee HN, Jeong MS, Jang SB. 'Oncogenic KRAS: Signaling and Drug Resistance', *Cancers*, vol. 13, no. 22, p. 5599, Nov. 2021, <https://doi.org/10.3390/cancers13225599>
- McCormick F. Sticking it to KRAS: covalent inhibitors enter the clinic. *Cancer Cell*. Jan. 2020;37(1):3–4. <https://doi.org/10.1016/j.ccell.2019.12.009>.
- Wittinghofer, Waldmann H. 'Ras—A Molecular Switch Involved in Tumor Formation', *Angew. Chem.*, vol. 39, no. 23, pp. 4192–4214, Dec. 2000, [https://doi.org/10.1002/1521-3773\(20001201\)39:23<4192::AID-ANIE4192>3.0.CO;2-Y](https://doi.org/10.1002/1521-3773(20001201)39:23<4192::AID-ANIE4192>3.0.CO;2-Y).
- Downward J. 'Targeting RAS signalling pathways in cancer therapy', *Nat. Rev. Cancer*, vol. 3, no. 1, pp. 11–22, Jan. 2003, <https://doi.org/10.1038/nrc969>
- Molina-Arcas M, Samani A, Downward J. 'Drugging the Undruggable: Advances on RAS Targeting in Cancer', *Genes*, vol. 12, no. 6, p. 899, Jun. 2021, <https://doi.org/10.3390/genes12060899>
- Brady DC, Hmeljak J, Dar AC. Understanding and drugging RAS: 40 years to break the tip of the iceberg. *Dis Model Mech*. Feb. 2022;15(2):dmm049519. <https://doi.org/10.1242/dmm.049519>
- Kessler D et al. Nov., 'Drugging all RAS isoforms with one pocket', *Future Med. Chem.*, vol. 12, no. 21, pp. 1911–1923, 2020, <https://doi.org/10.4155/fmc-2020-0221>
- Skoulidis F et al. Jun., 'Sotorasib for Lung Cancers with KRAS p.G12C Mutation', *N. Engl. J. Med.*, vol. 384, no. 25, pp. 2371–2381, 2021, <https://doi.org/10.1056/NEJMoa2103695>
- Wang X, et al. Identification of MRTX1133, a Noncovalent, Potent, and selective KRAS<sup>G12D</sup> inhibitor. *J Med Chem*. Feb. 2022;65(4):3123–33. <https://doi.org/10.1021/acs.jmedchem.1c01688>.
- Atanasov G, Zotchev SB, Dirsch VM, Supuran CT. 'Natural products in drug discovery: advances and opportunities', *Nat. Rev. Drug Discov.*, vol. 20, no. 3, pp. 200–216, Mar. 2021, <https://doi.org/10.1038/s41573-020-00114-z>
- Coy-Barrera E, Ogungbe IV, Schmidt TJ. 'Natural Products for Drug Discovery in the 21st Century: Innovations for Novel Therapeutics', *Molecules*, vol. 28, no. 9, p. 3690, Apr. 2023, <https://doi.org/10.3390/molecules28093690>
- Asiamah SA, Obiri W, Tamekloe FA, Armah, Borquaye LS. Applications of molecular docking in natural products-based drug discovery. *Sci Afr. Jul. 2023;20:e01593*. <https://doi.org/10.1016/j.sciaf.2023.e01593>.
- Pushpakom S, et al. Drug repurposing: progress, challenges and recommendations. *Nat Rev Drug Discov*. Jan. 2019;18(1):41–58. <https://doi.org/10.1038/nrd.2018.168>.
- Alamri MA, Alawam AS, Alshahrani MM, Kawsar SMA, Prinsa, Saha S. 'Establishing the Role of Iridoids as Potential Kirsten Rat Sarcoma Viral Oncogene Homolog G12C Inhibitors Using Molecular Docking; Molecular Docking Simulation; Molecular Mechanics Poisson–Boltzmann Surface Area; Frontier Molecular Orbital Theory; Molecular Electrostatic Potential; and Absorption, Distribution, Metabolism, Excretion, and Toxicity Analysis', *Molecules*, vol. 28, no. 13, p. 5050, Jun. 2023, <https://doi.org/10.3390/molecules28135050>
- Issahaku R et al. Jun., 'Discovery of Potential KRAS-SOS1 Inhibitors from South African Natural Compounds: An *In silico* Approach', *ChemistrySelect*, vol. 8, no. 24, p. e202300277, 2023, <https://doi.org/10.1002/slct.202300277>
- Lim TKH et al. Oct., 'KRAS G12C in advanced NSCLC: Prevalence, co-mutations, and testing', *Lung Cancer*, vol. 184, p. 107293, 2023, <https://doi.org/10.1016/j.lungcan.2023.107293>
- Wei D, Wang L, Zuo X, Maitra A, Bresalier RS. A small molecule with big impact: MRTX1133 targets the KRASG12D mutation in pancreatic Cancer. *Clin Cancer Res*. Nov. 2023;OF1–8. <https://doi.org/10.1158/1078-0432.CCR-23-2098>.
- van Santen, et al. The Natural products Atlas 2.0: a database of microbially-derived natural products. *Nucleic Acids Res*. Jan. 2022;50:D1317–23. <https://doi.org/10.1093/nar/gkab941>. no. D1.
- Schrödinger Release 2022-4: LigPrep*, Schrödinger, LLC, New York, NY, 2022.
- Shelley C, Cholletti A, Frye LL, Greenwood JR, Timlin MR, Uchimaya M. 'Epik: a software program for pK<sub>a</sub> prediction and protonation state generation for drug-like molecules', *J. Comput. Aided Mol. Des.*, vol. 21, no. 12, pp. 681–691, Dec. 2007, <https://doi.org/10.1007/s10822-007-9133-z>
- Schrödinger Release 2022-4: Protein Preparation Wizard*; Epik, Schrödinger, LLC, New York, NY, 2022; *Impact*, Schrödinger, LLC, New York, NY; *Prime*, Schrödinger, LLC, New York, NY, 2022.
- Madhavi Sastry G, Adzhigirey M, Day T, Annabhimoju R, Sherman W. 'Protein and ligand preparation: parameters, protocols, and influence on virtual screening enrichments', *J. Comput. Aided Mol. Des.*, vol. 27, no. 3, pp. 221–234, Mar. 2013, <https://doi.org/10.1007/s10822-013-9644-8>
- Lipinski CA. 'Drug-like properties and the causes of poor solubility and poor permeability', *J. Pharmacol. Toxicol. Methods*, vol. 44, no. 1, pp. 235–249, Jul. 2000, [https://doi.org/10.1016/S1056-8719\(00\)00107-6](https://doi.org/10.1016/S1056-8719(00)00107-6)
- Daina O, Michielin, Zoete V. 'SwissADME: a free web tool to evaluate pharmacokinetics, drug-likeness and medicinal chemistry friendliness of small molecules', *Sci. Rep.*, vol. 7, no. 1, p. 42717, Mar. 2017, <https://doi.org/10.1038/srep42717>
- Van Der Spoel D, Lindahl E, Hess B, Groenhof G, Mark AE, Berendsen HJC. 'GROMACS: Fast, flexible, and free', *J. Comput. Chem.*, vol. 26, no. 16, pp. 1701–1718, Dec. 2005, <https://doi.org/10.1002/jcc.20291>
- Lee J, et al. CHARMM-GUI Input Generator for NAMD, GROMACS, AMBER, OpenMM, and CHARMM/OpenMM simulations using the CHARMM36 Additive Force Field. *J Chem Theory Comput*. Jan. 2016;12(1):405–13. <https://doi.org/10.1021/acs.jctc.5b00935>.
- Vanommeslaeghe et al. 'CHARMM general force field: A force field for drug-like molecules compatible with the CHARMM all-atom additive biological force fields', *J. Comput. Chem.*, p. NA-NA, 2009, <https://doi.org/10.1002/jcc.21367>
- Berendsen HJC, Postma JPM, Van Gunsteren WF, DiNola A, Haak JR. 'Molecular dynamics with coupling to an external bath', *J. Chem. Phys.*, vol. 81, no. 8, pp. 3684–3690, Oct. 1984, <https://doi.org/10.1063/1.448118>
- Bussi G, Donadio D, Parrinello M. Canonical sampling through velocity rescaling. *J Chem Phys*. Jan. 2007;126(1):014101. <https://doi.org/10.1063/1.2408420>
- Bernetti, Bussi G. Pressure control using stochastic cell rescaling. *J Chem Phys*. Sep. 2020;153(11):114107. <https://doi.org/10.1063/5.0020514>.
- Darden T, York D, Pedersen L. 'Particle mesh Ewald: An *N* · log(*N*) method for Ewald sums in large systems', *J. Chem. Phys.*, vol. 98, no. 12, pp. 10089–10092, Jun. 1993, <https://doi.org/10.1063/1.464397>
- Hess B. A parallel Linear constraint Solver for Molecular Simulation. *J Chem Theory Comput*. Jan. 2008;4(1):116–22. <https://doi.org/10.1021/ct700200b>.

33. Kumar, Purohit R. 'Computational investigation of pathogenic nsSNPs in CEP63 protein', *Gene*, vol. 503, no. 1, pp. 75–82, Jul. 2012, <https://doi.org/10.1016/j.gene.2012.04.032>
34. Singh R, Purohit R. Computational analysis of protein-ligand interaction by targeting a cell cycle restrainer. *Comput Methods Programs Biomed. Apr.* 2023;231:107367. <https://doi.org/10.1016/j.cmpb.2023.107367>.
35. Bhardwaj VK, Purohit R. A comparative study on inclusion complex formation between formononetin and  $\beta$ -cyclodextrin derivatives through multi-scale classical and umbrella sampling simulations. *Carbohydr Polym. Jun.* 2023;310:120729. <https://doi.org/10.1016/j.carbpol.2023.120729>.
36. Bhardwaj V, Singh R, Singh P, Purohit R, Kumar S. Elimination of bitter-off taste of stevioside through structure modification and computational interventions. *J Theor Biol. Feb.* 2020;486:110094. <https://doi.org/10.1016/j.jtbi.2019.11.0094>.
37. Turner PJ, 'XMGRACE. Version 5.1. 19'. Center for Coastal and Land-Margin Research, Oregon Graduate Institute of Science and Technology, Beaverton, OR 2 (2005).
38. Humphrey W, Dalke A, Schulten K, 'VMD. Feb.:', 'Visual molecular dynamics', *J. Mol. Graph.*, vol. 14, no. 1, pp. 33–38, 1996, [https://doi.org/10.1016/0263-7855\(96\)00018-5](https://doi.org/10.1016/0263-7855(96)00018-5)
39. Grant BJ, Rodrigues APC, ElSawy KM, McCammon JA, Caves LSD. 'Bio3d: an R package for the comparative analysis of protein structures', *Bioinformatics*, vol. 22, no. 21, pp. 2695–2696, Nov. 2006, <https://doi.org/10.1093/bioinformatics/btl461>
40. Liu K, Watanabe E, Kokubo H. 'Exploring the stability of ligand binding modes to proteins by molecular dynamics simulations', *J. Comput. Aided Mol. Des.*, vol. 31, no. 2, pp. 201–211, Feb. 2017, <https://doi.org/10.1007/s10822-016-0005-2>
41. Durrant JD, McCammon JA. Molecular dynamics simulations and drug discovery. *BMC Biol. Dec.* 2011;9(1):71. <https://doi.org/10.1186/1741-7007-9-71>.
42. Zhang Z et al. Oct., 'GTP-State-Selective Cyclic Peptide Ligands of K-Ras(G12D) Block Its Interaction with Raf', *ACS Cent. Sci.*, vol. 6, no. 10, pp. 1753–1761, 2020, <https://doi.org/10.1021/acscentsci.0c00514>
43. Ajmal, et al. Prospective virtual screening combined with bio-molecular simulation enabled identification of new inhibitors for the KRAS drug target. *BMC Chem. Mar.* 2024;18(1):57. <https://doi.org/10.1186/s13065-024-01152-z>.
44. Zhou X, Ji Y, Zhou J. 'Multiple Strategies to Develop Small Molecular KRAS Directly Bound Inhibitors', *Molecules*, vol. 28, no. 8, p. 3615, Apr. 2023, <https://doi.org/10.3390/molecules28083615>
45. Canon J et al. Nov., 'The clinical KRAS(G12C) inhibitor AMG 510 drives anti-tumour immunity', *Nature*, vol. 575, no. 7781, Art. no. 7781, 2019, <https://doi.org/10.1038/s41586-019-1694-1>
46. Fell JB et al. Jul., 'Identification of the Clinical Development Candidate MRTX849, a Covalent KRAS<sup>G12C</sup> Inhibitor for the Treatment of Cancer', *J. Med. Chem.*, vol. 63, no. 13, pp. 6679–6693, 2020, <https://doi.org/10.1021/acscimedchem.9b02052>
47. Hallin J, et al. The KRASG12C inhibitor MRTX849 provides insight toward Therapeutic susceptibility of KRAS-Mutant cancers in Mouse models and patients. *Cancer Discov. Jan.* 2020;10(1):54–71. <https://doi.org/10.1158/2159-8290.CD-19-1167>.
48. Spencer-Smith R et al. Jan., 'Inhibition of RAS function through targeting an allosteric regulatory site', *Nat. Chem. Biol.*, vol. 13, no. 1, pp. 62–68, 2017, <https://doi.org/10.1038/nchembio.2231>
49. Mao Z, et al. KRAS(G12D) can be targeted by potent inhibitors via formation of salt bridge. *Cell Discov. Jan.* 2022;8(1). <https://doi.org/10.1038/s41421-021-00368-w>.
50. Ostrem JM, Peters U, Sos ML, Wells JA, Shokat KM. 'K-Ras(G12C) inhibitors allosterically control GTP affinity and effector interactions', *Nature*, vol. 503, no. 7477, pp. 548–551, Nov. 2013, <https://doi.org/10.1038/nature12796>
51. Lito P, Solomon M, Li L-S, Hansen R, Rosen N. Allele-specific inhibitors inactivate mutant KRAS G12C by a trapping mechanism. *Science. Feb.* 2016;351(6273):604–8. <https://doi.org/10.1126/science.aad6204>.
52. Cox D, Fesik SW, Kimmelman AC, Luo J, Der CJ. 'Drugging the undruggable RAS: Mission Possible?', *Nat. Rev. Drug Discov.*, vol. 13, no. 11, pp. 828–851, Nov. 2014, <https://doi.org/10.1038/nrd4389>
53. Patricelli P, et al. Selective inhibition of oncogenic KRAS output with small molecules targeting the inactive state. *Cancer Discov. Mar.* 2016;6(3):316–29. <https://doi.org/10.1158/2159-8290.CD-15-1105>.
54. Gerber M, Goel S, Maitra R. In silico comparative analysis of KRAS mutations at codons 12 and 13: structural modifications of P-Loop, switch I&II regions preventing GTP hydrolysis. *Comput Biol Med. Feb.* 2022;141:105110. <https://doi.org/10.1016/j.combiomed.2021.105110>.
55. Pantzar T. KRAS(G12C)–AMG 510 interaction dynamics revealed by all-atom molecular dynamics simulations. *Sci Rep. Jul.* 2020;10(1):11992. <https://doi.org/10.1038/s41598-020-68950-y>.
56. Issahaku R, et al. Characterization of the binding of MRTX1133 as an avenue for the discovery of potential KRASG12D inhibitors for cancer therapy. *Sci Rep. Oct.* 2022;12(1):17796. <https://doi.org/10.1038/s41598-022-22668-1>.
57. Liang F et al. Mar., 'Inhibition mechanism of MRTX1133 on KRASG12D: a molecular dynamics simulation and Markov state model study', *J. Comput. Aided Mol. Des.*, vol. 37, no. 3, pp. 157–166, 2023, <https://doi.org/10.1007/s10822-023-00498-1>
58. Lu S, Jang H, Nussinov R, Zhang J. The structural basis of oncogenic mutations G12, G13 and Q61 in small GTPase K-Ras4B. *Sci Rep. Feb.* 2016;6(1):21949. <https://doi.org/10.1038/srep21949>.

## Publisher's note

Springer Nature remains neutral with regard to jurisdictional claims in published maps and institutional affiliations.